AGU PUBLICATIONS

JGR

Journal of Geophysical Research: Atmospheres

RESEARCH ARTICLE

10.1002/2014JD022430

Key Points:
- COS and volcanic injections of SO_2 explain most of stratospheric aerosol
- Simulated radiative forcing consistent with estimates from observations
- All eruptions detected by MIPAS should be considered

Correspondence to:
C. Brühl,
christoph.bruehl@mpic.de

Citation:
Brühl, C., J. Lelieveld, H. Tost, M. Höpfner, and N. Glatthor (2015), Stratospheric sulfur and its implications for radiative forcing simulated by the chemistry climate model EMAC, *J. Geophys. Res. Atmos.*, *120*, 2103–2118, doi:10.1002/2014JD022430.

Received 25 AUG 2014
Accepted 3 FEB 2015
Accepted article online 9 FEB 2015
Published online 12 MAR 2015

Stratospheric sulfur and its implications for radiative forcing simulated by the chemistry climate model EMAC

C. Brühl[1], J. Lelieveld[1,2], H. Tost[3], M. Höpfner[4], and N. Glatthor[4]

[1] Atmospheric Chemistry Department, Max Planck Institute for Chemistry, Mainz, Germany, [2] Also at The Cyprus Institute, Nicosia, Cyprus, [3] Institute for Physics of the Atmosphere, Johannes Gutenberg University, Mainz, Germany, [4] Institute for Meteorology and Climate Research, Karlsruhe Institute of Technology, Karlsruhe, Germany

Abstract Multiyear simulations with the atmospheric chemistry general circulation model EMAC with a microphysical modal aerosol module at high vertical resolution demonstrate that the sulfur gases COS and SO_2, the latter from low-latitude and midlatitude volcanic eruptions, predominantly control the formation of stratospheric aerosol. Marine dimethyl sulfide (DMS) and other SO_2 sources, including strong anthropogenic emissions in China, are found to play a minor role except in the lowermost stratosphere. Estimates of volcanic SO_2 emissions are based on satellite observations using Total Ozone Mapping Spectrometer and Ozone Monitoring Instrument for total injected mass and Michelson Interferometer for Passive Atmospheric Sounding (MIPAS) on Envisat or Stratospheric Aerosol and Gases Experiment for the spatial distribution. The 10 year SO_2 and COS data set of MIPAS is also used for model evaluation. The calculated radiative forcing of stratospheric background aerosol including sulfate from COS and small contributions by DMS oxidation, and organic aerosol from biomass burning, is about 0.07 W/m^2. For stratospheric sulfate aerosol from medium and small volcanic eruptions between 2005 and 2011 a global radiative forcing up to 0.2 W/m^2 is calculated, moderating climate warming, while for the major Pinatubo eruption the simulated forcing reaches 5 W/m^2, leading to temporary climate cooling. The Pinatubo simulation demonstrates the importance of radiative feedback on dynamics, e.g., enhanced tropical upwelling, for large volcanic eruptions.

1. Introduction

Of all atmospheric sulfur species, carbonyl sulfide (COS) is the most abundant one [*Montzka et al.*, 2007], which is caused by biogenic and anthropogenic sources and its comparatively long atmospheric lifetime of more than 2 years. Due to this lifetime, about 0.15 Mt S yr^{-1} can enter the stratosphere at the tropical tropopause [*Brühl et al.*, 2012]. In contrast to sulfur dioxide (SO_2), which hydrolyzes and reacts in the aqueous phase, COS has a low solubility in cloud- and rainwater, limiting scavenging by clouds and precipitation. *Brühl et al.* [2012] also supported the original perception by *Crutzen* [1976] that the oxidation of COS into sulfate, contributing about 0.04 Mt S yr^{-1}, is the major source of the stratospheric background aerosol layer. Because the chemical conversion proceeds mostly about 10 km above the tropopause, a considerable fraction of COS (0.11 Mt S yr^{-1}) is transported back to the troposphere in the lower branch of the Brewer Dobson circulation. The presence of COS in the stratosphere is corroborated by satellite observations [e.g., *Barkley et al.*, 2008; *Leyser*, 2013], and its distribution is reproduced by model simulations [e.g., *Brühl et al.*, 2012; *English et al.*, 2011].

Hofmann et al. [2009] proposed that the observed increasing trend since about 2000 in stratospheric aerosol is due to increasing anthropogenic SO_2 emissions from China; however, *Vernier et al.* [2011], *Neely et al.* [2013], and also this study demonstrate that SO_2 injections from small- and medium-strength tropical volcanic eruptions and upward transport by the Brewer Dobson circulation can explain the observed increase in recent years. The almost 10 years of SO_2 observations by the Michelson Interferometer for Passive Atmospheric Sounding (MIPAS) on the European Environmental Satellite (Envisat) support this, indicated by the near absence of localized maxima in the lower stratosphere of the northern subtropics apart from volcanic eruptions [*Höpfner et al.*, 2013].

This article presents calculations with a coupled atmospheric chemistry general circulation model from the surface to the mesosphere and a comparison of the results with satellite data to study the stratospheric sulfur cycle and its relation to radiative and dynamical processes. After describing the MIPAS SO_2 data and

the model setup, the source gas COS for background aerosol is evaluated. The following section addresses simulated and observed SO_2 and its different sources. Finally, simulated stratospheric aerosol and its radiative effects, including comparison with observationally based studies, are presented. This includes the major Pinatubo eruption in 1991 for which many observations are available [e.g., *Read et al.*, 1993; *Wong et al.*, 2006; *Arfeuille et al.*, 2013], and several modeling studies that include aerosol microphysics have been performed [e.g., *English et al.*, 2013; *Aquila et al.*, 2012; *Toohey et al.*, 2011].

2. MIPAS SO_2 Observations

Two different versions of SO_2 retrievals from MIPAS in the period from July 2002 to April 2012 exist. The first version has been obtained from monthly and zonally (10° bands) averaged spectra [*Höpfner et al.*, 2013]. This data set has been optimized for a large altitude coverage comprising nearly the whole stratosphere from 15 to 45 km, albeit with limited horizontal and temporal resolution. Estimated errors are around 10–20 pptv with an altitude resolution of about 3.5–4 km at 20 km altitude up to 6–10 km at 40 km altitude [*Höpfner et al.*, 2013]. The second data set of SO_2, optimized for detection of volcanic enhancements, is obtained from single MIPAS limb scans [*Höpfner et al.*, 2015]. The retrieval of this new data set has been performed based on the standard processing scheme at the Institute for Meteorology and Climate Research which has been used to derive temperature and global trace gas distributions of more than 20 atmospheric constituents [*von Clarmann et al.*, 2003, 2009]. This data set covers the altitude range from about 10 to 22 km with the full horizontal and temporal resolution of the MIPAS observations. The vertical resolution varies from about 3 km at the lower end up to 5 km at the upper end of the profiles with estimated errors of about 80–150 pptv. As shown in *Höpfner et al.* [2015], the predominant error source for the single profile retrievals is spectral noise while other uncertainties contribute by about 10–70 pptv. Comparison of the MIPAS data set with independent satellite and in situ observations revealed a general consistency of better than 50 pptv for averaged profiles. Only directly after strong volcanic eruptions does MIPAS show systematically lower total values of SO_2 masses than observed by the Microwave Limb Sounder (MLS) on the Aura satellite [*Pumphrey et al.*, 2015]. This is attributed to the obstruction of infrared radiation in the limb path due to high concentrations of volcanic aerosol and ash and saturation of the signal in the IR spectrum caused by large amounts of SO_2. Two to four weeks after the eruption the SO_2 masses of MIPAS and MLS converge. Thus, volcanic emissions of SO_2 are likely to be underestimated when using MIPAS distributions directly after the eruption but can be corrected by extrapolation from observations some time after the eruption. This is described in greater detail by *Höpfner et al.* [2015].

3. Model Setup

In this study we present two simulations for the MIPAS period (July 2002 to December 2011), one where all volcanic eruptions detectable by MIPAS are considered and one with relatively large eruptions only. Also, we analyze a simulation for Pinatubo (July 1991 to December 1993).

We have used the ECHAM5 general circulation model [*Roeckner et al.*, 2006], coupled to the Modular Earth Submodel System (MESSy) [*Jöckel et al.*, 2006] Atmospheric Chemistry (EMAC) model, including the aerosol module GMXe [*Pringle et al.*, 2010; *Brühl et al.*, 2012] with seven aerosol modes (nucleation mode and soluble and insoluble Aitken, accumulation and coarse modes). The spectral model resolution applied is T42 (Triangular truncation at wavenumber 42 for spherical harmonics), i.e., about 2.8° in latitude and longitude. The vertical grid for the lower and middle atmosphere has 90 layers from the surface to a top layer centered at 0.01 hPa [*Giorgetta et al.*, 2006]. This model system generates an internally consistent Quasi-Biennial Oscillation (QBO), being close to the observations for up to the first 11 years analyzed (one MIPAS simulation), although the temporal agreement is partly coincidental. We did not apply data assimilation (i.e., nudging to actual meteorology) except for the initialization year 1996 (1990 for the Pinatubo simulation), and therefore the temporal agreement with actual meteorological phenomena such as the QBO deteriorates in 2007 and subsequent years (or even earlier in other simulations not shown in detail).

Mixing ratios of COS [*Montzka et al.*, 2007] and other long-lived source gases at the surface are taken from observations as in *Brühl et al.* [2012]. Lower boundary conditions for the different aerosol types (sulfate, nitrate, ammonium, organic and black carbon, mineral dust, sea salt, and aerosol water) are as described in *Pringle et al.* [2010], mostly based on AEROCOM (AEROsol interCOMparison project) emissions [*Dentener et al.*, 2006] and interactive calculations by the model. Anthropogenic trace gas emissions, including SO_2,

are taken from EDGAR (Emission Database for Global Atmospheric Research, http://www.pbl.nl/edgar/emission_data/edgar_32ft2000).

SO_2 emissions from outgassing volcanoes (i.e., volcanoes emitting into the lower and middle troposphere over longer time periods) are included as climatological sources. Volcanic SO_2 from explosive eruptions is injected into the stratosphere using the SO_2 masses derived from OMI (Ozone Monitoring Instrument) or TOMS (Total Ozone Mapping Spectrometer) satellite data from the NASA SO_2 database (http://so2.gsfc.nasa.gov) and the vertical and latitudinal distribution of MIPAS SO_2 5 day averages of individual retrievals [*Höpfner et al.*, 2015]. The lowest altitudes of MIPAS data considered are dependent on latitude (see Table 1). Because MIPAS cannot detect fresh plumes as the field of view is obscured by ash and because of other data gaps, in most cases two to six subsequent 5 day periods are used for extrapolation of the spatially integrated injected SO_2 masses listed in Table 1 and the initial spatial SO_2 distribution. In some cases the masses have been scaled to be consistent with the OMI or TOMS data (representing an upper limit because they include a tropospheric fraction) or, if available, estimates from MLS observations [*Pumphrey et al.*, 2015] or the Smithsonian database (http://www.volcano.si.edu) from which also the names of smaller volcanoes are adopted. If no MIPAS SO_2 is available, SAGE II (Stratospheric Aerosol and Gases Experiment) (update of *Thomason and Peter* [2006]; *Thomason et al.* [2008]) aerosol is used to estimate the spatial distribution. For tropical volcanoes except Pinatubo, SO_2 is injected in a zonally uniform manner in the altitude and latitude region derived from satellite data; for the other volcanoes given in Table 1, SO_2 is injected using a triangular sawtooth function of longitude with the maximum at the longitude of the eruption and the latitudinal and vertical distribution as observed. By using SAGE aerosol for the estimate of the spatial distribution of the injected SO_2, the plume to some degree artificially spreads to a wider latitude and altitude range because of the transport during the aerosol formation time period. If masses are not given explicitly in the data set as for TOMS, they are estimated from the maximum SO_2 column and the perturbed area. In this case the uncertainty regarding the stratospheric fraction is substantial.

Oceanic DMS is included in the simulations for the MIPAS period since it contributes to lower stratospheric sulfur, using the marine boundary conditions of *Kettle and Andreae* [2000]. The most important source region is the western Pacific Ocean, notably because some of the DMS and its oxidation products are transported into the tropical upper troposphere by strong convection over the Pacific warm pool. In our chemical scheme DMS is not fully converted to SO_2, as a large fraction stays in the upper troposphere and lower stratosphere as methylsulfonic acid (MSA, up to about 60 pptv) which is removed by transport, heterogeneous processes, and deposition.

In the photolysis calculations the 11 year solar cycle is taken into account. To reproduce the MIPAS observations of SO_2 at altitudes above the Junge layer [*Höpfner et al.*, 2013], compared to the setup in *Brühl et al.* [2012], the photolysis rate of gaseous H_2SO_4 has been enhanced by assuming that in the spectral band at 966 nm given in *Vaida et al.* [2003] it has a quantum yield of 20%. Additionally, a sink for sulfur by heterogeneous reactions on meteoric dust was introduced. We assume a uniform first-order sink of 2.4×10^{-8} s^{-1} based on the tropical meteoritic dust surface area densities of *Bardeen et al.* [2008] and an assumed sticking coefficient of 0.01 for gaseous H_2SO_4 (confirmed by *Saunders et al.* [2012]). As in *Brühl et al.* [2012], sedimentation of aerosol particles is calculated with a modified Walcek scheme described by *Benduhn and Lawrence* [2013].

Aerosol extinction is calculated based on Mie theory using precalculated look-up tables for the six aerosol components water, water-soluble species (including sulfuric acid and sulfate aerosol), organic carbon, black carbon, mineral dust, and sea salt in the Aitken, accumulation, and coarse modes. The radiation module can be used to perform additional diagnostic calculations of radiative forcing and heating rate anomalies for different aerosol options like the following: no aerosol, aerosol climatology or interactive aerosol, distinction between tropospheric and stratospheric aerosol, or different aerosol models. This allows, for example, to calculate the radiative forcing by stratospheric aerosol online by taking the differences between fluxes calculated with and without stratospheric aerosol. The boundary between the accumulation and coarse modes was shifted from 1.0 [*Brühl et al.*, 2012] to 1.6 μm to remedy the overestimation of sedimentation by large particles (a too large fraction in the coarse mode) for the Pinatubo case. Nevertheless, the tropospheric burdens of the different aerosol types and the total aerosol optical depth remain close to those calculated and evaluated by *Pringle et al.* [2010].

Table 1. Volcanic SO_2 Injections Into the Stratosphere, Estimated From TOMS/OMI, SAGE (Before 1994), and MIPAS (After July 2002) Satellite Data[a]

Volcano or Region	Time	Latitude	Longitude	Altitude (km)	SO_2 Mass (kt)
Pinatubo	15 Jun 1991	15	120	24	17,000
C. Hudson	9 Aug 1991	−45	−73	17	1,300
Spurr	27 Jun 1992	61	−152	16	900[b]
Spurr	18 Aug 1992	61	−152	16	900[b]
Lascar	19 Apr 1993	−23	−68	17	300
Ruang	26 Sep 2002	2	125	18	70[c,d]
Reventador	5 Nov 2002	0	−80	19	49[c,d]
Rabaul+Mayon	10 Mar 2003	−5, 13	150, 124	17,15	15[e]
Ulawun	9 Apr 2003	−5	151	17	18[e]
Anatahan	14 May 2003	16	143	17	16[e]
Soufriere Hills	13 Jul 2003	16	−62	15–18	51[d]
Gamalama+Japan	22 Aug 2003	1, 33	128, 131	16	27
Lokon+Masaya	26 Sep 2003	2, 12	125, −86	16	16
Manam?	21 Oct 2003	5	145	16	16
Philippines?	10 Nov 2003	5	120	16	20[e]
Colombia? MIPAS	25 Dec 2003	5	−78	17	13
Manam? MIPAS	9 Jan 2004	−5, 5	140?	17	27
Langila	3 Feb 2004	−5	150	17	14
Soufriere Hills	4 Mar 2004	10	−62	17	22[e]
Anatahan	12 Apr 2004	16	143	15	28
Pacaya	16 Jul 2004	15	−91	17	31
Manam	31 Oct 2004	−4	144	17	25[d]
Manam	24 Nov 2004	−4	144	17	35
Manam	28 Jan 2005	−4	144	19	169[c,d]
Anatahan	3 Apr 2005	16	143	15	15
Anatahan + Soufriere Hills	23 Apr 2005	16	143, −62	16	50[d]
Anatahan + Fernandina	17 May 2005	16, 0	143, −91	15	27[d]
Anatahan	12 Jun 2005	16	143	15	25
Anatahan + Santa Ana	12 Jul 2005	16	143, −90	15	26[d]
Anatahan + Conception	5 Aug 2005	16	143, −85	15	42
Anatahan	16 Aug 2005	16	143	15	59[d]
Sierra Negra	23 Oct 2005	−1	−91	15	48[d]
Karthala	24 Nov 2005	−10	43	16	28
Tinakula +	23 Jan 2006	−9	152	16	15
Ulawun	1 Mar 2006	−5	150	17	68[e]
Tinakula + Lascar	18 Apr 2006	−5, −23	152, −68	17	35
Soufriere Hills	21 May 2006	16	−62	19	147[c,d]
Ulawun + Ecuador	16 Jul 2006	−5	150, −80	17	20
Rabaul	17 Aug 2006	−4	150	19	88[e]
Rabaul	9 Oct 2006	−4	150	17	150[d]
Peru (?) + Pit.Fourn.R.	24 Oct 2006	−20, −10	−70, 57	17	48
Ambrym	8 Nov 2006	−10	160	17	40
Nyamuragira	28 Nov 2006	5, −15	30	17, 15	66[d]
Sulawesi + Japan	24 Dec 2006	5, 30	125	18, 15	34
Nevado del Huila	19 Feb 2007	0	−70	16	23
Pit.Fourn.R + Reventador +	3 Apr 2007	−20, 0	57, −80	16	52[d]
Ulawun + Vanuatu	3 May 2007	−5, −25	160	15	21
Vanuatu, Japan + Kam.	13 May 2007	−15, 35	150	16	25[e]
Llaima +	23 May 2007	−25–15	−70	15	25
Lengai +?	2 Jul 2007	−2, 20	29	16, 15	22
Raung, Monsoon?	27 Jul 2007	−5, 35	110	15	23[d]
Manda Hararo	11 Aug 2007	15–35	40	15	32
Vanuatu +?	20 Sep 2007	−5	165?	16	22
Jebel al Tair	1 Oct 2007	15–40	42[f]	16	74[d]
Nicaragua	5 Nov 2007	15	−85	16	27
Soputan or Krakatau	14 Nov 2007	−5	110	15	35[e]
Talang (?)	9 Dec 2007	−5	100	16	24[d]
Mexico? Llaima	29 Dec 2007	5, −35	−75 ?	17	27[d]
Nevado del Huila	8 Jan 2008	1	−71	15	30
Ecuador, Mexico?	28 Jan 2008	−5, 15	−80?	16	32

Table 1. (continued)

Volcano or Region	Time	Latitude	Longitude	Altitude (km)	SO_2 Mass (kt)
Ecuador?	11 Feb 2008	−5	−80	16	28[d]
Vanuatu+	8 Mar 2008	−15, 5	167	16	23
Vanuatu+Africa(?)	28 Mar 2008	−15, 5	167	16	28
Bismarck A. + Egon	12 Apr 2008	−5, 5	152, 122	15	27
Mexico+ Chaiten	3 May 2008	15,−5,−35	−90, −70	16	22[d]
Mexico+Barren I.+Chaiten	12 May 2008	10, −35	−90, 90	16	29
Nicaragua? Soputan?	16 Jun 2008	5	−85, 125	16	38[e]
Okmok	13 Jul 2008	53	−168[f]	15	89[d]
Kasatochi	8 Aug 2008	52	−175[f]	13–17	376[d]
Colombia+Dallafilla	12 Nov 2008	5	−78, 40	17	89[d]
Ecuador+Kamchatka?	17 Dec 2008	5, 40	−80, 160	17, 15	35
Karangetang?	2 Jan 2009	2	125	17	29[e]
Indonesia?	27 Jan 2009	−5	100	16	26[e]
Ecuador+Villarrica	16 Feb 2009	−5, −35	−75	16	28
Redoubt	23 Mar 2009	60	−155[f]	13	105[d]
Fernandina+	8 Apr 2009	0	−90	16	28[d]
Rinjani ?	7 May 2009	5	120	15	28
Rinjani+Vanuatu?	22 May 2009	5, −15	116, 165	16	27[d]
Sarychev	14 Jun 2009	48	153[f]	16	562[d]
Vanuatu+Mayon	4 Oct 2009	−15, 25	165, 120	17	27[e]
Costa Rica?	24 Oct 2009	5	−83	16	26[e]
Ecuador? Langila?	3 Dec 2009	−5	−78, 148	17	29[d]
Nyamuragira + Tungurahua	2 Jan 2010	−5, 15	30, −75	16	30[d]
Turrialba?	17 Jan 2010	5	−82	16	29
Soufriere Hills	13 Feb 2010	16	−62	16–18	42[d]
Costa Rica	2 Apr 2010	9	−84	15	34
Tungurahua ?	2 May 2010	−5	−78	16	39[e]
Pacaya	1 Jun 2010	15	−91	17	49[d]
Ulawun +Costa Rica+Kuril	16 Jul 2010	−5, 20, 35	150, −83	16	32[d]
Karangetang, Nicaragua	10 Aug 2010	9, 35	128, −85	16	38
Galeras + Sinabung (?)	27 Aug 2010	5, 25	−77, 100	16	34[d]
Karangetang + America?	4 Oct 2010	5	128, −80	16	42[d]
Merapi	6 Nov 2010	−7	110	18	107[d]
Java, Ecuador, Villarrica	24 Dec 2010	−5, −35	110, −78	17	51
Villarrica + Java	7 Jan 2011	−45, −5	−75, 110	16	35[d]
Lokon-Empung, Planchon?	26 Feb 2011	5, −40	110, −75	16	36[d]
Rabaul + Merapi?	25 Mar 2011	−5	150, 107	15	27
Colombia? Karangetang	12 Apr 2011	5	−77, 128	16	22[d]
Tungurahua, Rabaul	2 May 2011	−3	−78, 150	16	38[d]
Grimsvötn + Rabaul	27 May 2011	65, −5	−20, 150?	14, 16	48[e]
Nabro	13 Jun 2011	10–55	41[f]	16–19	386[e]
Vanuatu (?)	19 Oct 2011	−15	165	16	24[d]
Nyamuragira?	13 Nov 2011	−2	29	16	31[d]

[a] SO_2 masses above 14 km in low latitudes, above 13 km in midlatitudes, and 12 km in high latitudes. The altitudes and latitudes refer to the maxima in the zonal mean "plume" in the MIPAS SO_2 data if available. On several days more than one volcano has to be considered. The SO_2 is injected at the listed days, in most cases based on the strongest signal(s) in OMI data, i.e., not necessarily the first day of an eruption. For eruptions lasting over a period of months or years this can be several days. Most volcano names are from the Smithsonian database (http://www.volcano.si.edu).

[b] Probably overestimated by about a factor of 2.

[c] Above 15 km only.

[d] Approximately as in other simulation.

[e] Strongly underestimated in other simulation.

[f] Longitudinal sawtooth function.

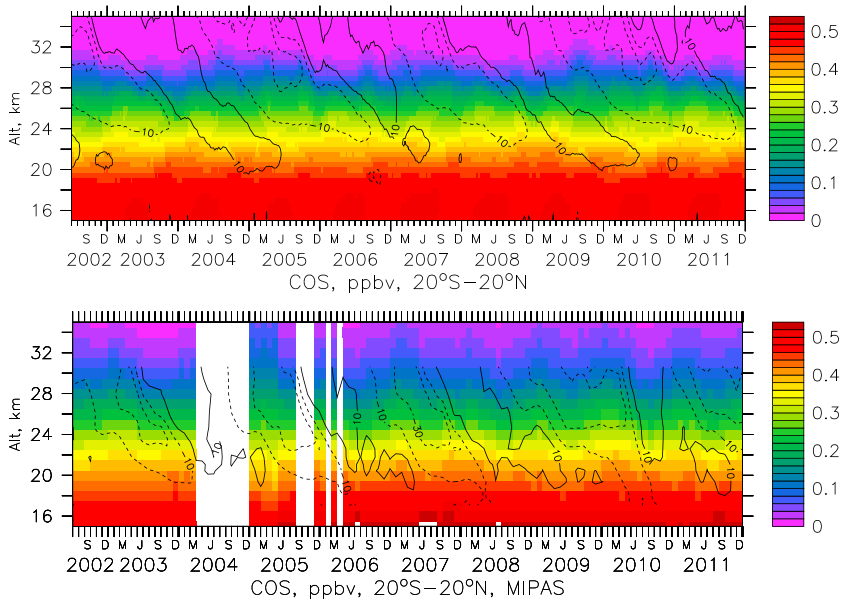

Figure 1. (top) EMAC simulated and (bottom) MIPAS observed COS in the tropics. Contours show the zonal wind in the 5°S–5°N latitude belt with increments of 20 m/s (QBO).

4. The Source Gas COS

Figure 1 shows the simulated vertical distribution of the main source gas COS for background stratospheric sulfur (top) together with corresponding MIPAS observations (bottom) [*Leyser*, 2013] in the tropics. The fastest decay with altitude due to photolysis occurs around 26 to 28 km. The amount of available COS for SO_2 formation is modulated by the QBO [*Leyser*, 2013; *Baldwin et al.*, 2001] with higher concentrations in the middle stratosphere during the easterly phase in both simulations and observations, due to enhanced upward transport. The overlaid contours in Figure 1 show the average zonal wind in the inner tropics as simulated (top) and as observed (bottom) over Singapore (http://www.geo.fu-berlin.de/en/met/ag/strat/produkte/qbo). As stated earlier, until about 2006 the simulated QBO is in phase with the observations, while later the phase is off due to a stall of the simulated east phase or easterly shear in 2007 (in the present simulation). The distribution of simulated COS with latitude agrees with observations, also shown in *Brühl et al.* [2012] by comparison with ACE/FTS (Atmospheric Chemistry Experiment/Fourier Transform Spectrometer) [*Barkley et al.*, 2008]. As analyzed by *Leyser* [2013], MIPAS and ACE/FTS observations are highly correlated, while MIPAS has the advantage of better coverage in the tropics. Above about 29 km MIPAS COS decreases less rapidly with altitude compared to the simulations, which is due to the averaging kernels for the rather low vertical resolution of about 10 km of the observations in this altitude range.

5. Simulated and Observed SO_2

5.1. The Envisat/MIPAS Period 2002–2011

Simulated and measured SO_2 for the period during which MIPAS observations [*Höpfner et al.*, 2013] have been performed are presented in Figure 2. In the upper stratosphere SO_2 increases with altitude due to the photolysis of gaseous H_2SO_4. There appears to be an interannual variability related to solar UV fluxes but also the semiannual oscillation of the zonal wind. In simulations and observations a secondary maximum around 28 km due to the production from COS photolysis can be recognized. This layer of SO_2 shows similar variations with the QBO as its source gas, i.e., relatively lower values during the westerly phases. The simulated maxima in the lower stratosphere due to the volcanic injections are larger than in the standard monthly average MIPAS data set [*Höpfner et al.*, 2013] because MIPAS data cannot be retrieved from areas with fresh plumes due to ash. If monthly averages are calculated from single retrievals [*Höpfner et al.*, 2015] as shown in Figure 2 (bottom), the volcanic signals are more pronounced. In contrast, the mean SO_2 background values at about 21 km altitude are around 20 pptv lower for the single retrievals compared to the average MIPAS data set and also somewhat lower than the simulations. We attribute this to systematic uncertainties in the single data set which is more suited for the analysis of high sulfur

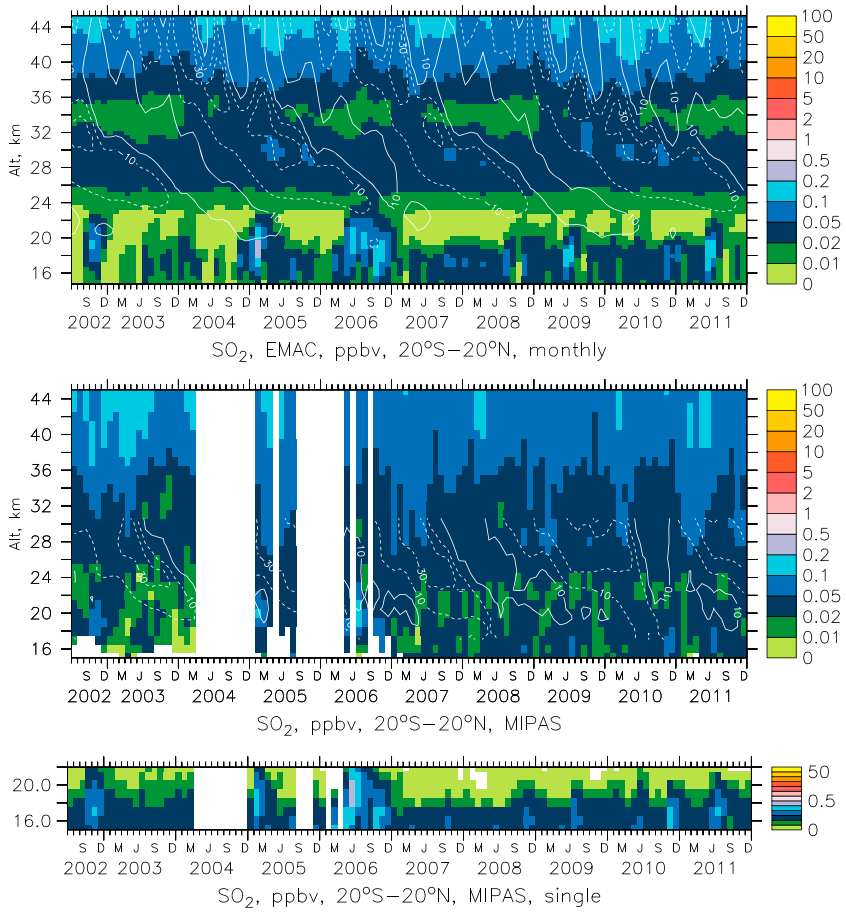

Figure 2. (top) Simulated and (middle) observed SO_2 in the tropics. (bottom) MIPAS data from individual retrievals for the lower stratosphere (same color scale, monthly averaged). Contours for QBO as in Figure 1.

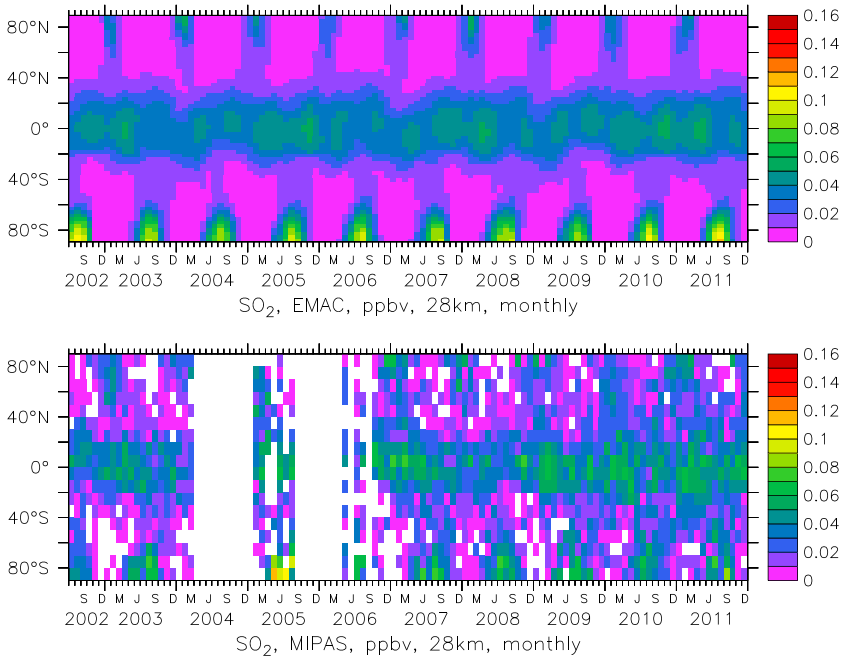

Figure 3. (top) Simulated and (bottom) observed SO_2 at 28 km altitude.

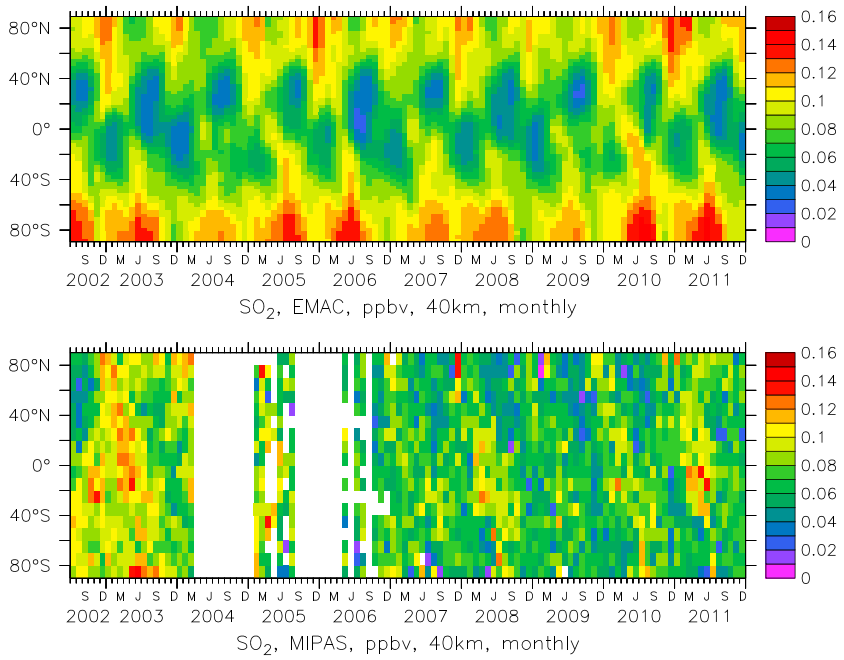

Figure 4. (top) Simulated and (bottom) observed SO_2 at 40 km altitude.

loadings related to volcanic eruptions and the plume dispersion than for a quantitative analysis of background SO_2 levels. In the lowermost tropical stratosphere (16–17 km) MIPAS observes background SO_2 concentrations of typically 20 to 50 pptv which can be simulated only if many more volcanoes are considered than listed in the NASA SO_2 database. Typical injections by these small- and medium-strength volcano eruptions derived from MIPAS and the Smithsonian database (direct or indirect via convective or advective transport) are of the order of 10 to 50 kt SO_2 (see Table 1). In addition, accounting for the oxidation of DMS helps to simulate realistic SO_2 concentrations in the lower tropical stratosphere in periods of low volcanic activity.

At 28 km (Figure 3) the source region from COS in low latitudes and the descent of SO_2 from the upper stratosphere in the high latitude winter can be identified, the latter being most pronounced over Antarctica. The observed distribution of SO_2 with latitude and season at 40 km (Figure 4) can be reproduced only by accounting for a sulfur sink on meteoric dust. Ignoring this process leads to a strong overestimate during high latitude winter (Figure 5, right). In spite of the observed SO_2 at 40 km being rather noisy, annual variability is detectable—similar to the model [see also *Höpfner et al.*, 2013, their Figure 6]. Further, the zonal mean distributions of SO_2 and the comparison with ATMOS data showed that the MIPAS SO_2 values at 40 km are robust within their estimated errors [*Höpfner et al.*, 2013, their Figures 7 and 9]. The conversion of SO_3 to H_2SO_4 is highly sensitive to temperature and the water vapor concentration [*Sander et al.*, 2011]. The small low bias in water vapor (about 0.5 ppmv (10%)) in this simulation leads to an overestimate of SO_2 at 40 km outside the tropics (Figure 4). At low latitudes it is necessary to include a contribution from near infrared

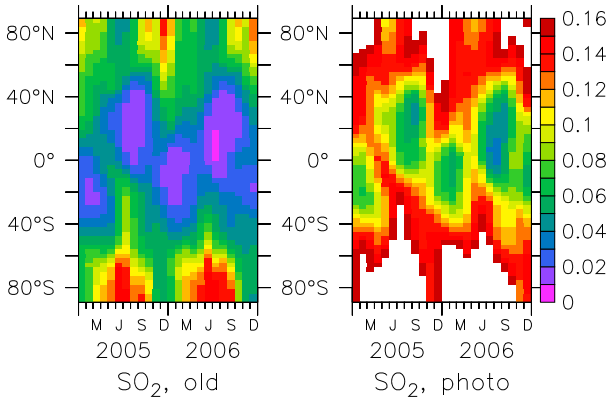

Figure 5. Simulated SO_2 at 40 km altitude (right) without meteoric dust sink and (left) additionally without enhanced H_2SO_4 photolysis. Typical subsets of longer simulations.

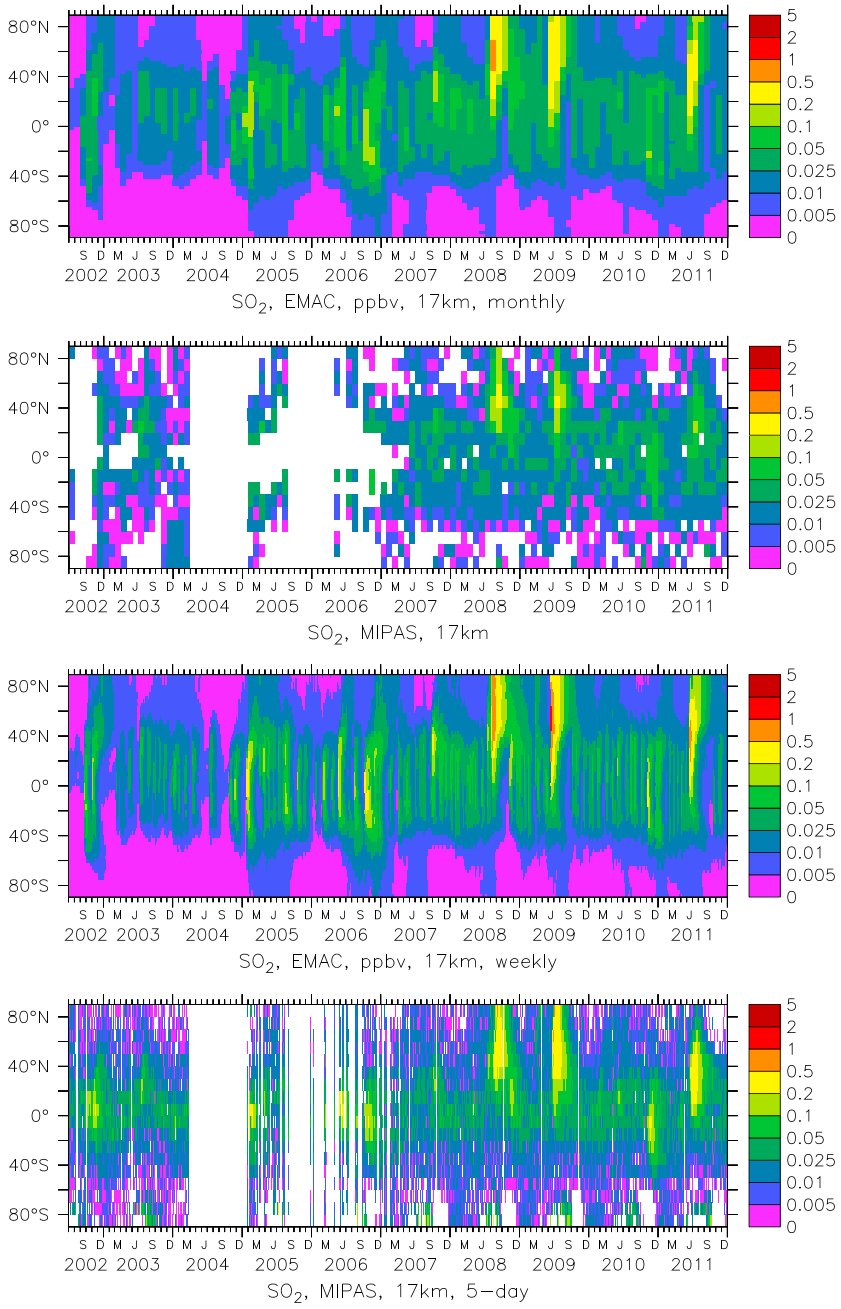

Figure 6. (first and third panels) Simulated and (second and fourth panels) observed SO_2 at 17 km altitude. Here MIPAS data are the monthly values of *Höpfner et al.* [2013] or 5 day averages of individual retrievals. As a general rule, each sudden increase in the observed or calculated SO_2 (Figure 6 third and fourth panels) is related to a volcanic eruption.

photolysis of gaseous H_2SO_4 to obtain agreement with the observations. Ignoring this causes calculated SO_2 to be about 50 pptv too low at 40 km (Figure 5, left).

5.2. Sensitivity to DMS and Anthropogenic SO_2

At 17 km the volcanic perturbations listed in Table 1 are clearly seen in simulation results and the MIPAS observations from individual retrievals (Figure 6). In periods with low volcanic activity like in 2004, the oxidation of DMS maintains an enhancement of 5 to 10 pptv in tropical SO_2 as shown by a sensitivity study ignoring DMS. Over the West Pacific the DMS contribution can be 20 pptv (Figure 7, first and second panels). This supports *Marandino et al.* [2013] who concluded that its contribution is small but nonnegligible. Anthropogenic emissions from China could potentially contribute a similar amount but are mostly

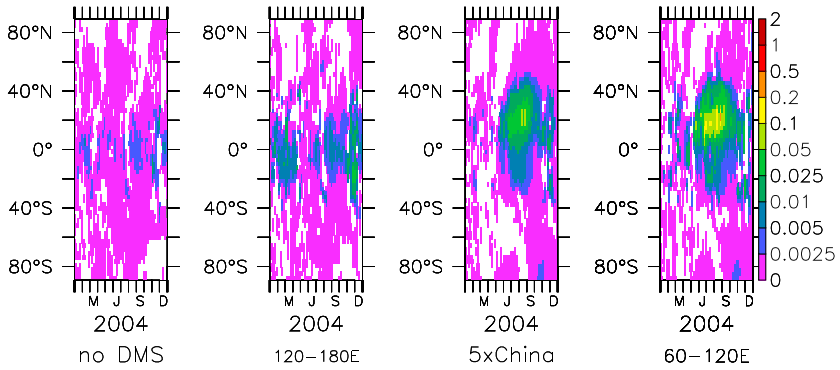

Figure 7. Simulated SO_2 changes in ppbv at 17 km altitude (first and second panels, reference simulation minus sensitivity study) without DMS and (third and fourth panels, sensitivity study minus reference of Figure 6) with 5 times the anthropogenic SO_2 emissions by China. In the white areas the values are slightly negative due to meteorological variability.

restricted to the Asian monsoon period. To clearly distinguish its signal, a sensitivity study with 5 times the EDGAR emissions from China was performed. Here an enhancement of about 50 pptv in zonal average during the monsoon period at about 25°N and up to 200 ppt between 60 and 120°E, but only a small effect in other seasons (Figure 7, third and fourth panels), was calculated. This pattern with local enhancements of up to 40 ppt with actual emissions cannot be clearly distinguished from noise or volcanic effects in the MIPAS observations. The calculated enhancement of stratospheric aerosol optical depth in August and September by 0.001 in the 30–50°N latitude belt is consistent with the simulations on increased Chinese and Indian emissions by *Neely et al.* [2013] though somewhat smaller.

5.3. The Pinatubo Eruption

For the Pinatubo simulation the injected SO_2 mass of 17 Mt [*Guo et al.*, 2004] is assumed to be distributed with altitude and latitude similar to the SAGE aerosol about 2 weeks after the eruption. Figure 8 shows that in the simulations SO_2 is lofted by the Brewer Dobson circulation and by radiative heating due to the aerosol (see below), leading to strongly enhanced SO_2 mixing ratios in the upper stratosphere and the mesosphere. This is consistent with ATMOS observations [*Rinsland et al.*, 1995], indicating 0.4 ppb in April 1992 and 0.2 ppb in April 1993 at 42 km. Figure 8 (right) allows a direct comparison with Figure 2 of *Rinsland et al.* [1995] as the model results are sampled in similar latitude and time ranges. Additionally, a typical background profile for the northern subtropics is included for the same season and QBO phase as the observations from SPACELAB in 1985. For all three periods EMAC agrees well with ATMOS in the altitude range between 33 and 50 km.

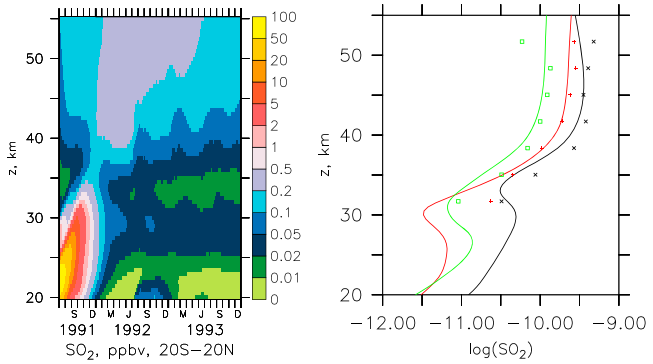

Figure 8. (left) Simulated SO_2 after Pinatubo, tropics. (right) Simulated SO_2 volume mixing ratios (decadal logarithm, lines) sampled as the three ATMOS campaigns of *Rinsland et al.* [1995] (symbols): black, ATLAS 1 (April 1992); red, ATLAS 2 (April 1993); and green, SPACELAB (May 1985; model here background of 2004 with same QBO phase as 1985).

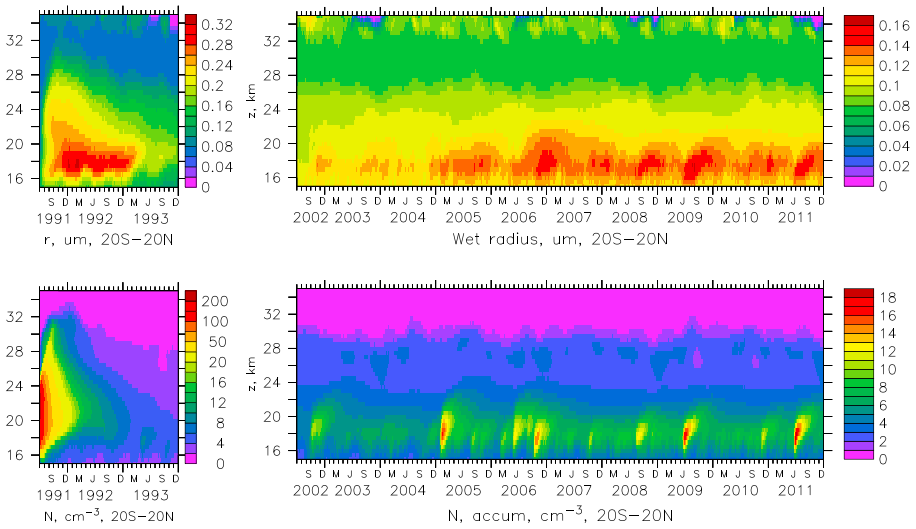

Figure 9. Aerosol number (top) median radius and (bottom) concentration in the accumulation mode. The mode boundary of 0.07 μm is the minimum value for the radius (left) Pinatubo and (right) MIPAS period.

6. Stratospheric Aerosol and Its Radiative Effects

6.1. Size Distribution, Mixing Ratios, and Extinction

Even for the large amount of SO_2 injected by Pinatubo, after about 1 month of simulation most of the SO_2 is converted to sulfate aerosol particles. For Pinatubo some particles grow into the coarse mode (up to 0.002 cm^{-3}) and sediment quickly. For the small- and medium-strength volcanic eruptions this does not happen as the lower concentration of precursor gases prevents the particles from growing into similarly large sizes. The simulated number median radius and number concentration in the dominating accumulation mode during the Pinatubo and MIPAS periods are given in Figure 9. For Pinatubo the number median radius is up to about 0.3 μm, for the medium volcanoes up to 0.16 μm, and for the background aerosol (e.g., summer 2002 or some other periods prior to 2005) slightly less than 0.1 μm (or 0.41, 0.22 and 0.14 μm area weighted effective radius for σ=1.49). This size range is consistent with volume distributions derived from in situ aircraft measurements from 1992 to 2004 by *Wilson et al.* [2008]. *Bingen et al.* [2004] found for Pinatubo a number median radius up to 0.55 μm using a monomodal distribution, which seems consistent with our results also taking into account the coarse mode fraction. In the background Junge layer a significant part of sulfate aerosol is present in the Aitken mode.

For Pinatubo several sensitivity studies have been performed varying the mode boundaries and distribution widths. For example, using the mode boundary of *Brühl et al.* [2012] for the coarse mode would result in about 10 times more particles in the coarse mode and a much smaller number median radius in the accumulation mode (0.2 μm) because of more efficient removal of particulate mass by sedimentation. This leads to reduction of the aerosol residence time and stratospheric aerosol optical depth by about a factor of 2. Using a mode boundary of 1.8 μm instead of 1.6 μm would slightly increase the residence time of Pinatubo aerosol and particle size in accumulation mode, as suggested by observations, but would lead to unrealistic model results in the troposphere. Note that for the background stratospheric aerosol and the medium-strength volcanic eruptions the settings of the mode boundary for the coarse mode are not relevant.

In our chemistry climate model the prognostic tracers, including sulfate aerosol, are represented as volume mixing ratios to maintain mass conservation. The total volume mixing ratio of simulated sulfate aerosol, i.e., the sum of the four soluble modes, is shown in Figure 10 for the tropics. In Figure 10 (right) the Junge layer is distinctly visible at about 28 km altitude, modulated by the QBO following COS and SO_2 with higher values during the east phase [*Hommel et al.*, 2014]. The lower stratospheric aerosol is strongly enhanced by the tropical volcanic eruptions after October 2002. Also, the two rather strong midlatitude eruptions in 2008 and 2009 contributed significantly to stratospheric aerosol in the tropics. For Pinatubo (Figures 10 (left) and 11 (left) for the corresponding optical depth) the presence of coarse mode particles causes faster decay than observed, demonstrating that in this case the seven-mode aerosol model is at its limit and a multisize bin model, though computationally demanding, might be more appropriate. The timing and the altitude

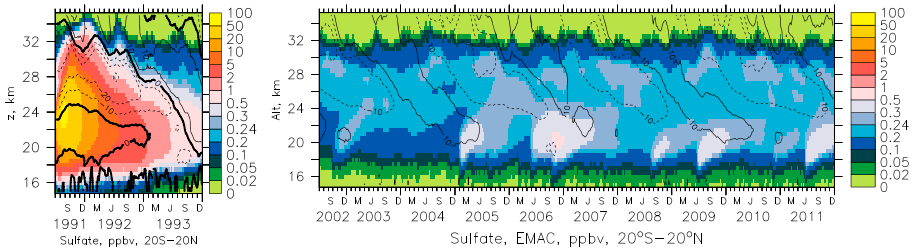

Figure 10. Simulated total sulfate aerosol volume mixing ratio, tropics. Contours, QBO as in Figure 1 (additional contours on the left).

of the peak and the lofting of the aerosol to more than 30 km are simulated in close agreement with the observations by SAGE [*Thomason and Peter*, 2006], using the conversion formula (surface area density to volume mixing ratio) of *Grainger et al.* [1995].

The calculated zonal mean total stratospheric aerosol optical depth (AOD) at 530 nm is shown in Figure 11. For the Pinatubo case our results in the tropics and the Northern Hemisphere are close to those observed and the model simulation results of *English et al.* [2013], *Toohey et al.* [2011], and *Aquila et al.* [2012]. In our model more volcanic aerosol spreads to the Southern Hemisphere than in the results of *English et al.* [2013], closer to observations. The optical depth peaks at 0.52 in August 1991. For the small- and medium-strength eruptions it is more than an order of magnitude less. Here Kasatochi (2008) and Sarychev (2009) have the strongest local contributions, while Rabaul (2006) causes a global perturbation. The simulation with all eruptions listed in Table 1 agrees well with estimates from satellites in the tropics (Figure 11, middle) [*Santer et al.*, 2014], except for 2004 and 2007 where the sizes and number of volcanic injections appear to be underestimated. Ignoring smaller volcanoes (i.e., using only the ones marked with superscripted letters d and e in Table 1) leads to strong underestimate of stratospheric optical depth after 2003. Organic carbon

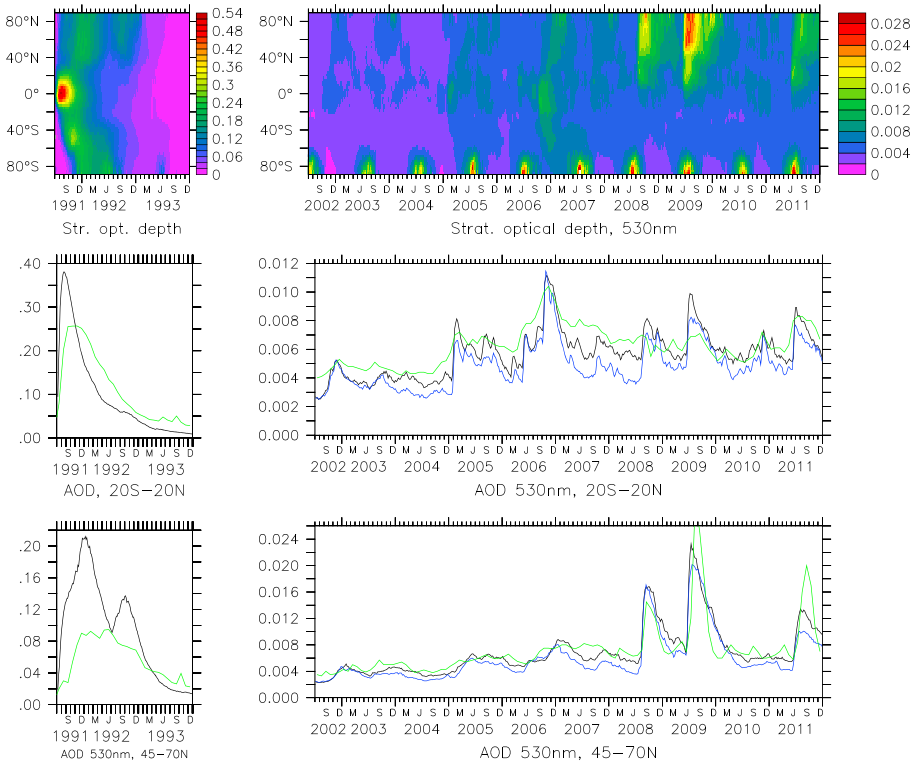

Figure 11. Aerosol optical depth at 530 nm above 185 hPa. The green lines show values derived from SAGE+CALIPSO (middle) and SAGE+OSIRIS (bottom) satellite observations, the black lines the simulations using the SO_2 injections of Table 1, and the blue lines the simulation with a reduced number of small volcanoes as marked in the last column of Table 1. Data gaps in the SAGE data for Pinatubo are filled similar to *Arfeuille et al.* [2013].

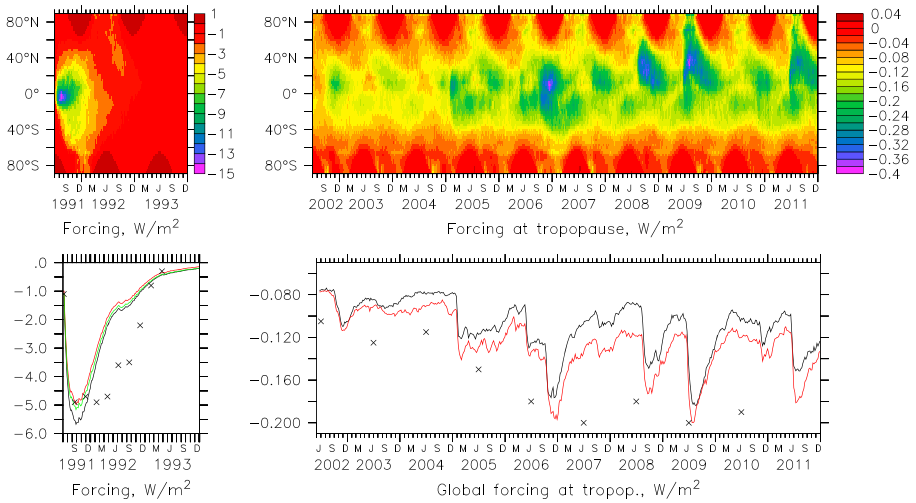

Figure 12. Radiative forcing at the tropopause (185 hPa, solar + IR) by stratospheric aerosol. Estimates from observations for global forcing (bottom row) are indicated by crosses [*Toohey et al.*, 2011; *Solomon et al.*, 2011], to be compared with the red curves. The ERBE data for Pinatubo (left column) are for solar forcing at the top of the atmosphere. In the bottom left the green and the black curves are the total and solar forcing at the tropopause, respectively. The black curve in the bottom right is the reduced volcanic SO_2 simulation also shown in Figure 11.

contributes about 10% to the AOD in the tropics with local peaks near the biomass burning regions and during the Asian monsoon (for observations, see, e.g., *Borrmann et al.* [2010]). For Pinatubo the EMAC model overestimates optical depth in the first 4 months after the eruption compared to SAGE, while for a later period the model underestimates it because of too fast (coarse) particle removal. This effect is much larger than the influence of QBO-related variability. However, in the first 8 months after the eruption the SAGE data have large uncertainty because of a data gap in the lower stratosphere due to saturation which has to be filled by extrapolations. For high latitudes (Figure 11, bottom) there are no SAGE observations in winter due to the lack of sunlight. The secondary maximum in 1992 in the simulations due to the eruption of Spurr appears to be overestimated (overestimated uncertain emissions, Table 1). In the 2002 to 2011 period the EMAC simulation of optical depth agrees well with OSIRIS observations [*Bourassa et al.*, 2012]. The explicit simulation of the Grimsvötn eruption and a better extrapolation of the MIPAS data for Nabro helps to reduce the underestimate in the summer of 2011.

6.2. Radiative Heating and Climate Forcing

The extinction by aerosol exerts a radiative forcing at the tropopause of up to 0.4 W/m^2 for the medium-strength volcanoes (solar+IR) and 13 W/m^2 for Pinatubo (Figure 12). This corresponds to a forcing of up to 0.15 W/m^2 in global annual average for 2009 (0.14 W/m^2 for 2006 and 2007), which is slightly lower (about 0.02 to 0.04 W/m^2) compared to that derived from observations [*Solomon et al.*, 2011], and about 5 W/m^2 (or 6 W/m^2 solar only and 5 W/m^2 solar only at top of the atmosphere) for the Pinatubo case (Figure 12, bottom row). The latter agrees with that derived from the Earth Radiation Budget Experiment (ERBE) [*Wong et al.*, 2006; *Toohey et al.*, 2011]. The forcing exerted by volcanoes in the 2002 to 2011 period strongly depends on the number of eruptions considered. Using only the volcanoes marked with superscripted letters d and e in Table 1 reduces the mean forcing perturbation by more than 0.02 W/m^2.

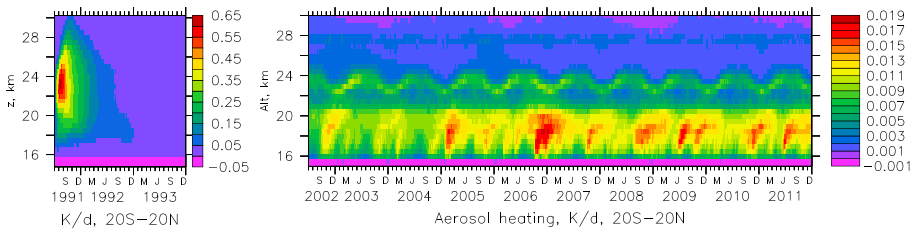

Figure 13. Aerosol total radiative heating, tropics.

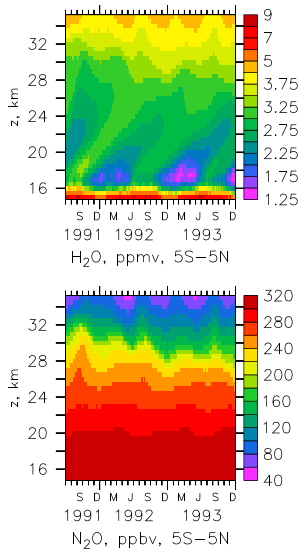

Figure 14. EMAC simulated lofting of trace gases H_2O and N_2O due to aerosol heating.

Absorption of solar near-infrared and terrestrial infrared radiation causes a radiative heating of the stratospheric aerosol layer. For volcanic sulfur aerosol the contributions from both spectral regions are about the same in the tropics. For sulfur aerosol the contribution to radiative heating in the visible part of the spectrum is small. We find that in the regions of the lower stratosphere affected by pollution via the Asian and African monsoons, absorption of visible solar radiation by black and organic carbon [e.g., *Murphy et al.*, 2013] also contributes to radiative heating. As can be seen from Figure 13 aerosol from volcanoes like Soufriere Hills and Rabaul exerts a heating of 0.02 K/d, while for Pinatubo the effect is about 30 times larger.

6.3. Feedback on Dynamics

The radiative heating of Pinatubo aerosol induces enhanced tropical upwelling and a lofting of chemical tracers, including N_2O, water vapor, the aerosol itself, and the injected SO_2 (Figures 14, 10, and 8). A more detailed analysis of dynamical consequences including enhanced wave activity is presented by *Toohey et al.* [2014]. Ignoring the radiative feedback on dynamics would reduce the aerosol extinction in the upper part of the volcanic aerosol plume (28 km in September 1991 descending to 24 km 1 year later) by more than 50% as shown by a sensitivity simulation. Without feedback on dynamics the calculated absolute global forcing in 1992 would be about 0.3 W/m^2 less in average and still 0.1 W/m^2 less in 1993 compared to Figure 12. For water vapor in the first 6 months after the eruption the tropical tape recorder is accelerated, and N_2O shows a spike between 25 and 32 km (Figure 14) which is similar to the perturbation calculated by *Aquila et al.* [2012]. Similar to the observations, the radiative perturbation appears to cause a stall of the easterly phase or shear of the QBO [*Labitzke*, 1994; *Aquila et al.*, 2014]; however, the variability in the duration of this stall is rather large as shown by sensitivity simulations. For the small- to medium-strength volcanic eruptions radiative heating causes a slight perturbation in temperature and the vertical wind for about 3 months following the eruptions (not shown). After that time it cannot be distinguished from the meteorological variability.

7. Conclusions

In our model calculations the transport of COS from the troposphere and volcanic injections of SO_2 into the stratosphere explain most of the observed stratospheric aerosol load, including trends, in agreement with SO_2 observations by MIPAS. Penetration of significant amounts of anthropogenic SO_2 from China into the stratosphere appears unlikely, apparent from the MIPAS data and the model results. The MIPAS data [*Höpfner et al.*, 2013, also unpublished data, 2015] and the simulations indicate, however, that also small- to medium-strength volcanic eruptions in the tropics have to be included in the model if they reach about 15 km. Especially in 2007, significant eruptions have taken place that are not represented in the NASA SO_2 database but can be estimated from the MIPAS data and the Smithsonian volcano list. However, in this year the optical depth and the radiative forcing is still underestimated by considering the listed volcanoes (Table 1), indicating that some eruptions are not yet identified. In our model calculations marine DMS contributes 5–10 pptv to SO_2 in the lower tropical stratosphere and should be included in simulations. Our results suggest that enhanced photolysis of H_2SO_4 and a meteoric dust sink for H_2SO_4 need to be accounted for to reproduce observations of SO_2 in the upper stratosphere and mesosphere. The global radiative forcing of up to about 0.2 W/m^2 (annual average) due to the sulfate aerosols caused by the medium-strength volcanoes since the early 2000s may have contributed to the observed slowdown of global warming in the past decade, corroborating similar conclusions by *Santer et al.* [2014], *Ridley et al.* [2014], and *Solomon et al.* [2011]. In the case of a major eruption like Pinatubo, radiative heating by stratospheric aerosol causes enhanced upwelling in the tropics leading to lofting of the sulfur species, long-lived tracer gases such as N_2O, and an accelerated H_2O tape recorder. For such eruptions the impact of aerosol and stratospheric chemistry feedbacks on dynamics is essential to achieve agreement with observations.

Acknowledgments
The computations have been performed at the blizzard supercomputer at DKRZ, Hamburg, Germany. At DKRZ detailed model output is also stored on tape and available through the authors. For the MIPAS data we refer to http://www.imk-asf.kit.edu/english/308.php. The sulfur injections from the volcanoes were estimated utilizing the NASA SO_2 database at GSFC (http://so2.gsfc.nasa.gov) and the Smithsonian volcano database (http://www.volcano.si.edu). The group of C. Bingen at BIRA, Belgium, provided the processed OSIRIS data for comparison. The research leading to these results has received funding from the European Research Council under the European Union's Seventh Framework Programme (FP7/2007–2013)/ERC grant agreement 226144.

References

Aquila, V., L. D. Oman, R. S. Stolarski, P. R. Colarco, and P. A. Newman (2012), Dispersion of the volcanic sulfate cloud from a Mount Pinatubo like eruption, *J. Geophys. Res.*, *117*, D06216, doi:10.1029/2011JD016968.

Aquila, V., C. I. Garfinkel, P. A. Newman, L. D. Oman, and D. W. Waugh (2014), Modifications of the quasi-biennial oscillation by a geoengineering perturbation of the stratospheric aerosol layer, *Geophys. Res. Lett.*, *41*, 1738–1744, doi:10.1002/2013GL058818.

Arfeuille, F., B. P. Luo, P. Heckendorn, D. Weisenstein, J. X. Sheng, E. Rozanov, M. Schraner, S. Brönnimann, L. W. Thomason, and T. Peter (2013), Modeling the stratospheric warming following Mt. Pinatubo eruption: Uncertainties in aerosol extinctions, *Atmos. Chem. Phys.*, *13*, 11,221–11,234, doi:10.5194/acp-13-11221-2013.

Baldwin, M. P., et al. (2001), The quasi-biennial oscillation, *Rev. Geophys.*, *39*, 179–229.

Bardeen, C. G., O. B. Toon, E. J. Jensen, D. R. Marsh, and V. L. Harvey (2008), Numerical simulations of the three-dimensional distribution of meteoric dust in the mesosphere and upper stratosphere, *J. Geophys. Res.*, *113*, D17202, doi:10.1029/2007JD009515.

Barkley, M. P., P. I. Palmer, C. D. Boone, P. F. Bernath, and P. Suntharalingam (2008), Global distributions of carbonyl sulfide in the upper troposphere and stratosphere, *Geophys. Res. Lett.*, *35*, L14810, doi:10.1029/2008GL034270.

Benduhn, F., and M. G. Lawrence (2013), An investigation of the role of sedimentation for stratospheric climate engineering, *J. Geophys. Res. Atmos.*, *118*, 7905–7921, doi:10.1002/jgrd.50622.

Bingen, C., D. Fussen, and F. Vanhellemont (2004), A global climatology of stratospheric aerosol size distribution parameters derived from SAGE II data over the period 1984–2000: 1. Methodology and climatological observations, *J. Geophys. Res.*, *109*, D06201, doi:10.1029/2003JD003518.

Borrmann, S., et al. (2010), Aerosols in the tropical and subtropical UT/LS: In-situ measurements of submicron particle abundance and volatility, *Atmos. Chem. Phys.*, *10*, 5573–5592, doi:10.5194/acp-10-5573-2010.

Bourassa, A. F., L. A. Rieger, N. D. Lloyd, and D. A. Degenstein (2012), Odin-OSIRIS stratospheric aerosol data product and SAGE III intercomparison, *Atmos. Chem. Phys.*, *12*, 605–614, doi:10.5194/acp-12-605-2012.

Brühl, C., J. Lelieveld, P. J. Crutzen, and H. Tost (2012), The role of carbonyl sulphide as a source of stratospheric sulphate aerosol and its impact on climate, *Atmos. Chem. Phys.*, *12*, 1239–1253, doi:10.5194/acp-12-1239-2012.

Crutzen, P. J. (1976), The possible importance of CSO for the sulphate layer of the stratosphere, *Geophys. Res. Lett.*, *3*, 73–76.

Dentener, F., et al. (2006), Emissions of primary aerosol and precursor gases in the years 2000 and 1750 prescribed data-sets for AeroCom, *Atmos. Chem. Phys.*, *6*, 4321–4344, doi:10.5194/acp-6-4321-2006.

English, J. M., O. B. Toon, M. J. Mills, and F. Yu (2011), Microphysical simulations of new particle formation in the upper troposphere and lower stratosphere, *Atmos. Chem. Phys.*, *11*, 9303–9322, doi:10.5194/acp-11-9303-2011.

English, J. M., O. B. Toon, and M. J. Mills (2013), Microphysical simulations of large volcanic eruptions: Pinatubo and Toba, *J. Geophys. Res. Atmos.*, *118*, 1880–1895, doi:10.1002/jgrd.50196.

Giorgetta, M. A., E. Manzini, E. Roeckner, M. Esch, and L. Bengtsson (2006), Climatology and forcing of the quasi-biennial oscillation in the MAECHAM5 model, *J. Clim.*, *19*, 3882–3901.

Grainger, R. G., A. Lambert, C. D. Rodgers, F. W. Taylor, and T. Deshler (1995), Stratospheric aerosol effective radius, surface area and volume estimated from infrared measurements, *J. Geophys. Res.*, *100*, 16,507–16,518.

Guo, S., G. J. S. Bluth, W. I. Rose, I. M. Watson, and A. J. Prata (2004), Re-evaluation of SO_2 release of the 15 June 1991 Pinatubo eruption using ultraviolet and infrared satellite sensors, *Geochem. Geophys. Geosyst.*, *5*, Q04001, doi:10.1029/2003GC000654.

Hofmann, D., J. Barnes, M. O'Neill, M. Trudeau, and R. R. Neely (2009), Increase in background stratospheric aerosol observed with lidar at Mauna Loa Observatory and Boulder, Colorado, *Geophys. Res. Lett.*, *36*, L15808, doi:10.1029/2009GL039008.

Höpfner, M., et al. (2013), Sulphur dioxide (SO_2) as observed by MIPAS/Envisat: Temporal development and spatial distribution at 15–45 km altitude, *Atmos. Chem. Phys.*, *13*, 10,405–10,423, doi:10.5194/acp-13-10405-2013.

Höpfner, M., et al. (2015), Sulfur dioxide (SO_2) from MIPAS in the upper troposphere and lower stratosphere 2002–2012, *Atmos. Chem. Phys. Discuss.*, *15*, 5801–5847, doi:10.5194/acpd-15-5801-2015.

Hommel, R., C. Timmreck, M. A. Giorgetta, and H. F. Graf (2014), Quasi-biennial oscillation of the tropical stratospheric aerosol layer, *Atmos. Chem. Phys. Discuss.*, *14*, 16243–16290, doi:10.5194/acpd-14-16243-2014.

Jöckel, P., et al. (2006), The atmospheric chemistry general circulation model ECHAM5/MESSy1: Consistent simulation of ozone from the surface to the mesosphere, *Atmos. Chem. Phys.*, *6*, 5067–5104, doi:10.5194/acp-6-5067-2006.

Kettle, A., and M. Andreae (2000), Flux of dimethylsulfide from the ocean: A comparison of updated data sets and flux models, *J. Geophys. Res.*, *105*, 26,793–26,808.

Labitzke, K. (1994), Stratospheric temperature changes after the Pinatubo eruption, *J. Atmosph. Terr. Phys.*, *56*(9), 1027–1034.

Leyser, R. K. A. (2013), Carbonylsulfid (OCS) aus MIPAS-Satellitendaten: Retrievalstrategie und Klimatologie, Diplomathesis, IMK, Karlsruhe Institute of Technology, Germany.

Marandino, C. A., S. Tegtmeier, K. Krüger, C. Zindler, E. L. Atlas, F. Moore, and H. Bange (2013), Dimethylsulphide (DMS) emissions from the West Pacific Ocean: A potential marine source for stratospheric sulphur, *Atmos. Phys. Chem.*, *13*, 8427–8437, doi:10.5194/acp-13-8427-2013.

Montzka, S. A., P. Calvert, B. D. Hall, J. W. Elkins, T. J. Conway, P. P. Tans, and C. Sweeney (2007), On the global distribution, seasonality, and budget of atmospheric carbonyl sulfide and some similarities with CO_2, *J. Geophys. Res.*, *112*, D09302, doi:10.1029/2006JD007665.

Murphy, D. M., K. D. Froyd, J. P. Schwarz, and J. C. Wilson (2013), Observations of the chemical composition of stratospheric aerosol particles, *Q. J. R. Meteorol. Soc.*, *140*, 1269–1278, doi:10.1002/qj.2213.

Neely, R. R., III et al. (2013), Recent anthropogenic increases in SO_2 from Asia have minimal impact on stratospheric aerosol, *Geophys. Res. Lett.*, *40*, 999–1004, doi:10.1002/grl.50263.

Pringle, K. J., H. Tost, S. Message, B. Steil, D. Giannadaki, A. Nenes, C. Fountoukis, P. Stier, E. Vignati, and J. Lelieveld (2010), Description and evaluation of GMXe: A new aerosol submodel for global simulations (v1), *Geosci. Model Dev.*, *3*, 391–412, doi:10.5194/gmd-3-391-2010.

Pumphrey, H. C., W. G. Read, N. J. Livesey, and K. Yang (2015), Observations of volcanic SO_2 from MLS on AURA, *Atmos. Meas. Tech.*, *8*, 195–209, doi:10.5194/amt-8-195-2015.

Read, W. G., L. Froidevaux, and J. W. Waters (1993), Microwave Limb Sounder measurements of stratospheric SO_2 from the Mt. Pinatubo volcano, *Geophys. Res. Lett.*, *20*, 1299–1302.

Ridley, D. A., et al. (2014), Total volcanic stratospheric aerosol optical depths and implications for global climate change, *Geophys. Res. Lett.*, *41*, 7763–7769, doi:10.1002/2014GL061541.

Rinsland, C. P., M. R. Gunson, M. K. W. Ko, D. W. Weisenstein, R. Zander, M. C. Abrams, A. Goldman, N. D. Sze, and G. K. Yue (1995), H_2SO_4 photolysis: A source of sulfur dioxide in the upper stratosphere, *Geophys. Res. Lett.*, *22*, 1109–1112.

Roeckner, E., R. Brokopf, M. Esch, M. Giorgetta, S. Hagemann, L. Kornblueh, E. Manzini, U. Schlese, and U. Schulzweida (2006), Sensitivity of simulated climate to horizontal and vertical resolution in the ECHAM5 atmosphere model, *J. Clim.*, *19*, 3771–3791.

Sander, S. P., et al. (2011), *Chemical Kinetics and Photochemical Data for Use in Atmospheric Studies, Evaluation Number 17*, JPL publication 10-6, Pasadena, Calif.

Santer, B. D., et al. (2014), Volcanic contribution to decadal changes in tropospheric temperature, *Nat. Geosci.*, *7*, 185–189, doi:10.1038/ngeo2098.

Saunders, R. W., S. Dhomse, W. S. Tian, M. P. Chipperfield, and J. M. C. Plane (2012), Interactions of meteoritic smoke particles with sulphuric acid in the Earth's stratosphere, *Atmos. Chem. Phys.*, *12*, 4337–4398, doi:10.5194/acp-12-4387-2012.

Solomon, S., J. S. Daniel, R. R. Neely III, J. P. Vernier, E. G. Dutton, and L. W. Thomason (2011), The persistently variable "background" stratospheric aerosol layer and global climate change, *Science*, *333*, 866–870.

Thomason, L. R., and T. Peter (eds.) (2006), *Assessment of Stratospheric Aerosol Properties (ASAP)*, SPARC Rep. 4, WRCP 124, WMO/TD No. 1295, Toronto, Canada. [Available at http://www.sparc-climate.org/publications/sparc-reports.]

Thomason, L. W., S. P. Burton, B.-P. Luo, and T. Peter (2008), SAGE II measurements of stratospheric aerosol properties at non-volcanic levels, *Atmos. Chem. Phys.*, *8*, 983–995, doi:10.5194/acp-8-983-2008.

Toohey, M., K. Krüger, U. Niemeier, and C. Timmreck (2011), The influence of eruption season on the global aerosol evolution and radiative impact of tropical volcanic eruptions, *Atmos. Chem. Phys.*, *11*, 12,351–12,367, doi:10.5194/acp-11-12351-2011.

Toohey, M., K. Krüger, M. Bittner, C. Timmreck, and H. Schmidt (2014), The impact of volcanic aerosol on the Northern Hemisphere stratospheric polar vortex: Mechanisms and sensitivity to forcing structure, *Atmos. Chem. Phys.*, *14*, 13,063–13,079, doi:10.5194/acp-14-13063-2014.

Vaida, V., H. G. Kjaergaard, P. E. Hintze, and D. J. Donaldson (2003), Photolysis of sulfuric acid vapor by visible solar radiation, *Science*, *299*, 1566–1568.

Vernier, J.-P., et al. (2011), Major influence of tropical volcanic eruptions on the stratospheric aerosol layer during the last decade, *Geophys. Res. Lett.*, *38*, L12807, doi:10.1029/2011GL047563.

von Clarmann, T., et al. (2003), Retrieval of temperature and tangent altitude pointing from limb emission spectra recorded from space by the Michelson Interferometer for Passive Atmospheric Sounding (MIPAS), *J. Geophys. Res.*, *108*, 4736, doi:10.1029/2003JD003602.

von Clarmann, T., et al. (2009), Retrieval of temperature, H_2O, O_3, HNO_3, CH_4, N_2O, $ClONO_2$ and ClO from MIPAS reduced resolution nominal mode limb emission measurements, *Atmos. Meas. Tech.*, *2*, 159–175.

Wilson, J. C., et al. (2008), Steady-state aerosol distributions in the extra-tropical, lower stratosphere and the processes that maintain them, *Atmos. Chem. Phys.*, *8*, 6617–6626, doi:10.5194/acp-8-6617-2008.

Wong, T., B. A. Wielicki, R. B. Lee III, G. L. Smith, K. A. Bush, and J. K. Willis (2006), Reexamination of the observed decadal variability of the Earth Radiation Budget using altitude-corrected ERBE/ERBS nonscanner WFOV data, *J. Clim.*, *19*, 4028–4040.